Hadronic Final State in DIS at low x at HERA

Vladimir Shekelyan (Chekelian)
DESY, Hamburg / ITEP, Moscow
H1 Collaboration

Abstract

Deep-inelastic scattering ($\gamma^* p$) interactions with photon virtualities $Q^2 > 5$ GeV^2 and photon-proton (γp) interactions with $Q^2 < 10^{-2}$ GeV^2 are studied at the high energy electron-proton collider HERA. The transverse energy flow and relative rates of large rapidity gap events are compared in the two event samples. The observed similarity between $\gamma^* p$ and γp interactions can be understood in a picture where the photon develops as a hadronic object. The transverse energy density measured in the central region of the collision, at $\eta^* = 0$ in the $\gamma^* p$ centre of mass frame, is compared with data from hadron-hadron interactions as function of the CMS energy of the collision.

Photon-proton processes are traditionally classified according to the virtuality (Q^2) of the photon. For quasi-real photoproduction interactions Q^2 is close to zero, and correspondingly the photon is nearly on mass shell. Interactions which involve a Q^2 larger than a few GeV^2 are usually termed deep-inelastic scattering processes (DIS). This distinction results mainly from the different theoretical descriptions adopted for these processes. Photoproduction has turned out to be very similar to hadron-hadron collisions and is described in a VMD-like (Vector Meson Dominance) picture, where the photon is assumed to fluctuate into a vector meson before interacting with the proton. For DIS on the other hand, the observation of scaling of the structure function in early experiments suggested that this interaction could, in the infinite momentum frame of the proton, be interpreted as a hard scattering process in which a point-like virtual photon "probes" the structure of the hadronic target. The subsequently measured scaling violations are well described by perturbative QCD.

However, recent DIS measurements at the high energy ep collider HERA and high precision measurements from fixed target leptoproduction experiments have shown that the data in the low Bjorken-x region reveal properties from soft low-p_T processes as seen in hadronic collisions as well. Here $x = Q^2/2P \cdot q$ where P and q are the four momenta of the incoming proton and photon, respectively. Elastic and other diffractive hadronic final states have been produced [1, 2] and shadowing on nuclear targets has been observed [3], phenomena which are well known from hadron-hadron and real photon collisions. These observations suggest that the different treatment of low and high Q^2 interactions is somewhat artificial, and it is therefore worthwhile testing a prescription which provides a natural transition between these two classes.

A qualitative approach for a smooth transition of the high energy $\gamma^* p$ [1] interactions over a large range of Q^2 results from viewing the photon-proton collision in the proton rest frame and the hypothesis that the photon can develop as a hadronic object before interacting with the nuclear target. The lifetime of a high energy real photon to fluctuate into a hadronic state is much longer than the time of the strong interaction itself, and therefore this picture is generally applied to describe photoproduction interactions. The same argument can be used for DIS interactions at low x. In the proton rest frame the time in which the virtual photon can fluctuate and stay in a hadronic state, e.g. a quark-antiquark pair, is given by $\tau \approx 1/(xM_p)$ [4, 5], where M_p is the mass of the nucleon target. Thus, for small x, the virtual photon can convert into a quark-antiquark pair and cover a distance which is long compared to the interaction length. For an x in the range of $10^{-2} - 10^{-4}$ this distance is in the range of 10 to 1000 fm, much larger than the typical radius of the target. Therefore, at low x, a virtual photon can stay in a hadronic state for a long time and interact with the target strongly, leading to a final state similar to the one in a hadron-hadron collision. Note that this is not in contradiction with the traditional treatment of DIS as a point-like process, where a virtual photon "probes" the hadronic structure of the nuclear target. In fact both pictures are taken to be complementary, as discussed in [5].

The HERA collider provides a unique opportunity to study the final state of both photoproduction and DIS interactions at high energy and small Bjorken-x: 26.7 GeV electrons collide with 820 GeV protons, yielding a centre of mass energy $\sqrt{s}$ of 296 GeV. This allows for a study of DIS interactions for x values down to $\sim 10^{-4}$, and photoproduction collisions at a centre of mass energy of $\sim$ 200 GeV. The data recorded with the H1 experiment are used to study the transverse energy behaviour in DIS interactions and photoproduction, and the analogy with hadronic collisions is checked. Within this analogy $\gamma^* p$ events can be sub-divided in rapidity-space into three regions, which differ in the mechanism by which the hadronic final state is produced [6]: the proton fragmentation region, the photon fragmentation region and

[1] In this paper the generic symbol γ^* is used to denote a colliding photon irrespective of the virtuality.

a hadron plateau spanning the rapidity interval between the two. The region of the hadronic plateau is expected to be independent of the nature of the two incoming "hadrons", as was verified in hadron-hadron collisions. The "hadronic" nature of the photon is assumed to change with increasing Q^2, thus the photon fragmentation region is expected to change with Q^2.

Also studied is the fraction of diffractive events in DIS and photoproduction. In hadronic collisions approximate factorization of the cross section for high mass diffractive dissociation has been observed, in accordance with Regge theory predictions [7]: the ratio of the hadron diffractive dissociation to the total cross section is found to be approximately independent of the type of dissociating hadron and is thus the same for pions, kaons, protons and real photons. Applying this factorization property to real and virtual photons leads to the expectation that the ratio of the photon diffractive dissociation cross section to the total cross section is independent of the Q^2 of the photon, in the high dissociative mass region.

The data used in this analysis were collected in 1993 and correspond to an integrated luminosity of about 0.3 pb^{-1}. The kinematic variables Q^2, x and y of the ep collision are determined from the scattered electron: $Q^2 = 4\,E_e\,E'_e \cos^2(\theta_e/2)$ and $y = 1-(E'_e/E_e)\cdot\sin^2(\theta_e/2)$, where E_e is the energy of the incident electron and E'_e and θ_e are the energy and the polar angle of the scattered electron respectively. The scaling variable x is then derived via $x = Q^2/(ys)$, and the total hadronic invariant mass is given by $W^2 = sy - Q^2$.

The hadronic energy flow and the scattered electrons in DIS processes are measured with a liquid argon (LAr) calorimeter and a backward electromagnetic lead-scintillator calorimeter (BEMC), which cover the polar angular range $4^\circ < \theta < 153^\circ$ and $151^\circ < \theta < 177^\circ$, respectively. θ is defined with respect to the proton beam direction ($+z$ axis). In the photoproduction sample of events the scattered electron is detected in the small angle electron detector, which is part of the luminosity system. Details on the scattered electron identification procedure in the BEMC ($5 < Q^2 < 100$ GeV^2) and LAr ($Q^2 > 100$ GeV^2) calorimeters and in the small angle electron detector ($Q^2 < 10^{-2}$ GeV^2, $0.3 < y < 0.5$) can be found in [8]. A detailed description of the H1 apparatus can be found in [9].

The data are corrected for detector effects using samples of Monte Carlo generated events which were fully simulated in the H1 detector. The PHOJET [10] generator for photoproduction and the CDM [11] (Colour Dipole Model) generator for DIS processes were used. To estimate systematic uncertainties of the correction procedure for DIS events another model for the hadronic final state was used as well: the MEPS (Matrix Elements plus Parton Showers) model [12].

Results

For comparisons of event properties at different Q^2 values, the $\gamma^* p$ centre of mass system (CMS) is chosen as frame of reference. The orientation of the CMS is such that the direction of the proton defines the positive z' axis. Transverse quantities are defined with respect to the proton direction in this frame.

The flow of transverse energy, E_T, as a function of pseudorapidity $\eta^* = -\ln(\tan\frac{\theta^*}{2})$ in the CMS is shown in Fig. 1. Here θ^* is the polar angle of a particle in the CMS frame with respect to the proton direction. The transverse energy is calculated from the energy deposits in the calorimeter cells. For this study the DIS data are restricted to the same kinematic region $0.3 < y < 0.5$ as the photoproduction events. The y range corresponds to a mean $\gamma^* p$ collision energy of $\sqrt{s_{\gamma p}} = W \approx 185$ GeV. The corrections which have been applied to correct for detector effects never exceed 30%.

Only statistical errors are shown in Fig. 1. For the comparison of the E_T spectra at the four different Q^2 values it is important to identify the relative systematic uncertainty, so the

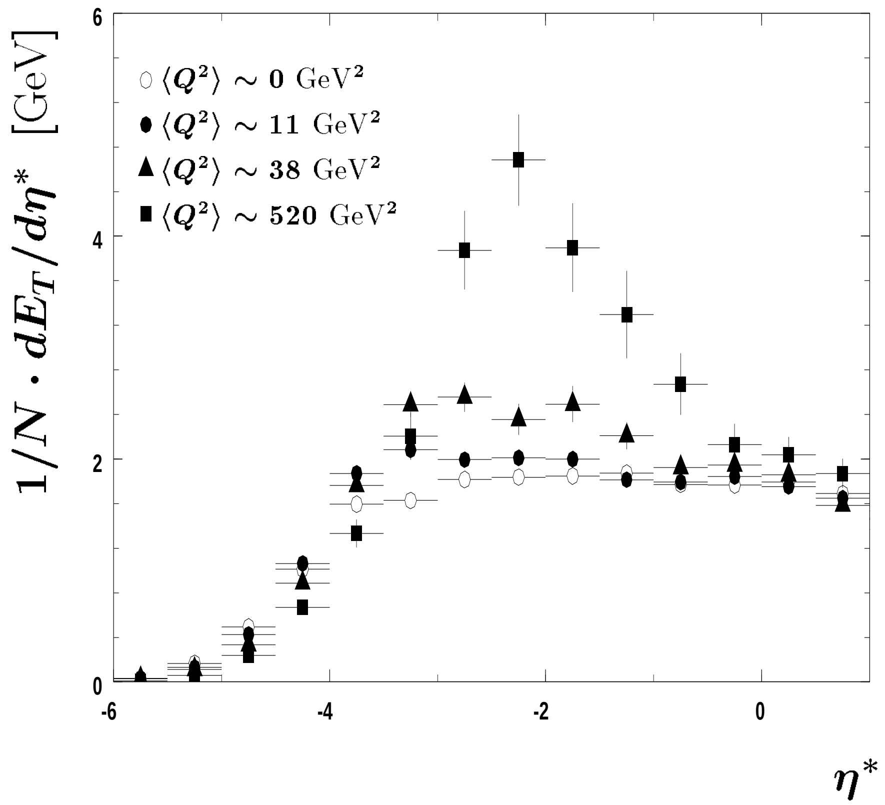

Figure 1: The flow of transverse energy E_T in the hadronic CMS as a function of pseudorapidity η^* normalized to the number of events N. Photoproduction data (open circles) are compared with DIS data (full symbols: circles – $\langle Q^2\rangle \approx 11$ GeV^2, triangles – $\langle Q^2\rangle \approx 38$ GeV^2, squares – $\langle Q^2\rangle \approx 520$ GeV^2) in the same y range $0.3 < y < 0.5$ ($W \approx 185$ GeV).

systematic errors on each "Q^2 point" at a given η^* value are considered in two parts. Firstly there is a point-to-point systematic error, which has a different effect on each of the four measurements, accounting for kinematically dependent systematic effects. Secondly there is an overall scale error which affects all four points at a given η^* value in the same way. The main source of the point-to-point systematic error is the model dependence of the correction for detector effects. This dependence was investigated with the CDM and MEPS models and leads to a point-to-point error of 6%. Additionally, the model dependence contributes 6% to the overall scale error at each η^* value. Further contributions to the overall scale error arise from the LAr and BEMC calorimeter calibration (5% and 20% respectively), and from details of the analysis method, such as the calorimeter noise treatment, the clustering scheme for the calorimeter cells, and the accuracy of the simulation of the calorimeter response, affecting the results by 5% in the region close to the proton direction ($\eta^* > -1$). All these contributions give an overall scale error varying from 8% in the photon fragmentation region ($-3.5 < \eta^* < -1$) to 9% in the central region ($\eta^* > -1$), and up to 20% in the region $\eta^* < -3.5$, which does not affect the results of the present analysis. This discussion on the systematic errors is also valid for data shown below.

Fig.1 demonstrates that the transverse energy flow exhibits a strong increase in the photon fragmentation region ($\eta^* < -1$), from $Q^2 = 0$ (photoproduction) to $Q^2 \approx 500$ GeV^2 (DIS), while in the central region the level of E_T remains almost the same. Such behaviour is expected if the central region corresponds to the hadronic plateau, discussed in the introduction. In order to quantify the change of E_T with Q^2, the value of E_T per unit of pseudorapidity (E_T density)

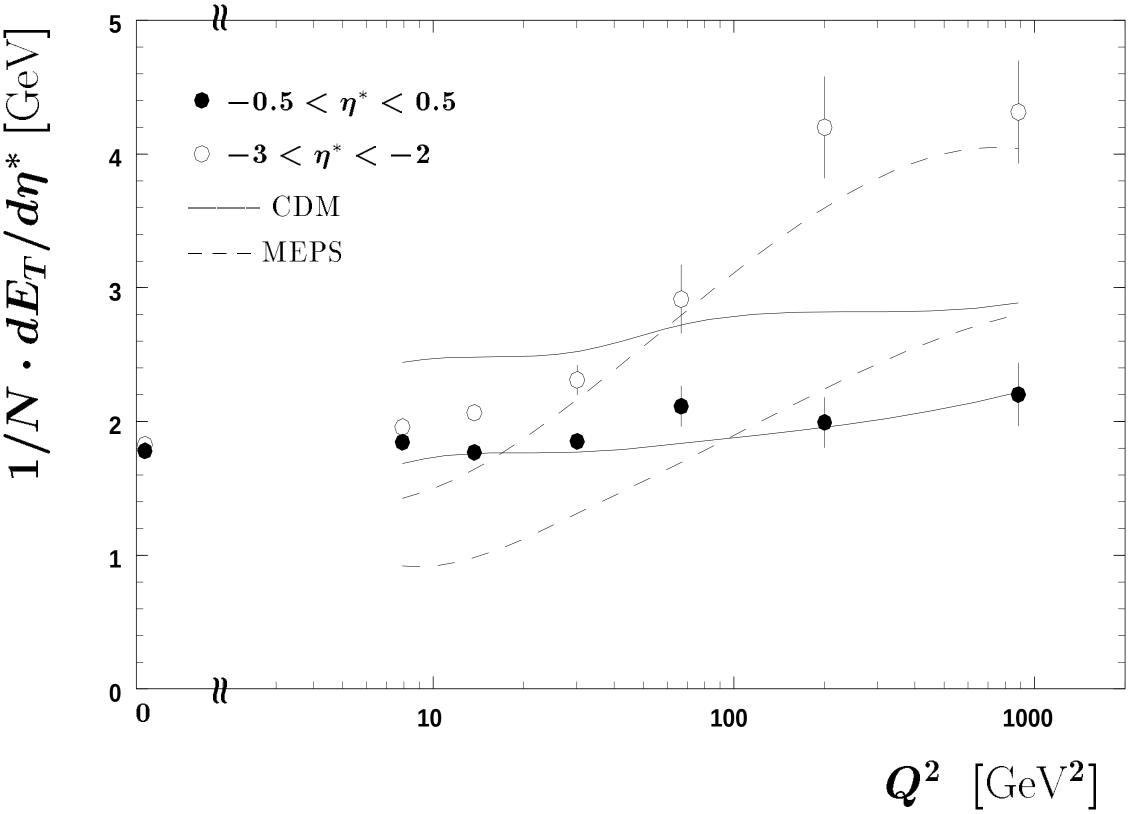

Figure 2: The transverse energy per unit of pseudorapidity in the CMS central region ($-0.5 < \eta^* < 0.5$, full circles) and in the photon fragmentation region ($-3 < \eta^* < -2$, open circles) as a function of Q^2 for $0.3 < y < 0.5$. For comparison, the CDM (full line) and MEPS (dashed line) models are shown. The lower curves correspond to the CMS central region and the upper ones to the photon fragmentation region.

for an η^* slice in the central pseudorapidity region ($-0.5 < \eta^* < 0.5$) and an η^* slice in the photon fragmentation region ($-3 < \eta^* < -2$) is shown in Fig. 2. The data clearly demonstrate that the transverse energy in the central region is essentially independent of the Q^2 of the photon, but increases significantly in the photon fragmentation region.

In Fig. 2 the results are compared with predictions from the CDM and MEPS models. The E_T density predicted by the CDM model is found to be independent of Q^2, which is in accordance with the data in the central region, but does not reproduce the data in the photon fragmentation region. The MEPS model on the other hand describes the behaviour of the transverse energy flow in the photon fragmentation region but fails in the central region. The comparison of absolute values of the E_T density between the data and models should be viewed with some caution since diffractive events are not included in these models. These events, which amount to $\approx 6\%$ of all events, give rise to a rapidity gap [1], i.e. no energy deposition in the central region. The exclusion of diffractive events however does not change the shape of the distribution of the E_T density versus Q^2. Comparisons of the energy flows for models and data with rapidity gap events removed can be found in [13].

Within the hadronic picture, the observation of a rise of the E_T density with Q^2 in the photon fragmentation region implies that, on arrival at the target, the virtual photon has a hadronic structure (parton configuration) which depends on Q^2. With increasing Q^2 the transverse momentum of the constituent partons in this hadronic structure increases. A formal explanation of this effect based on QCD calculations is given in [14].

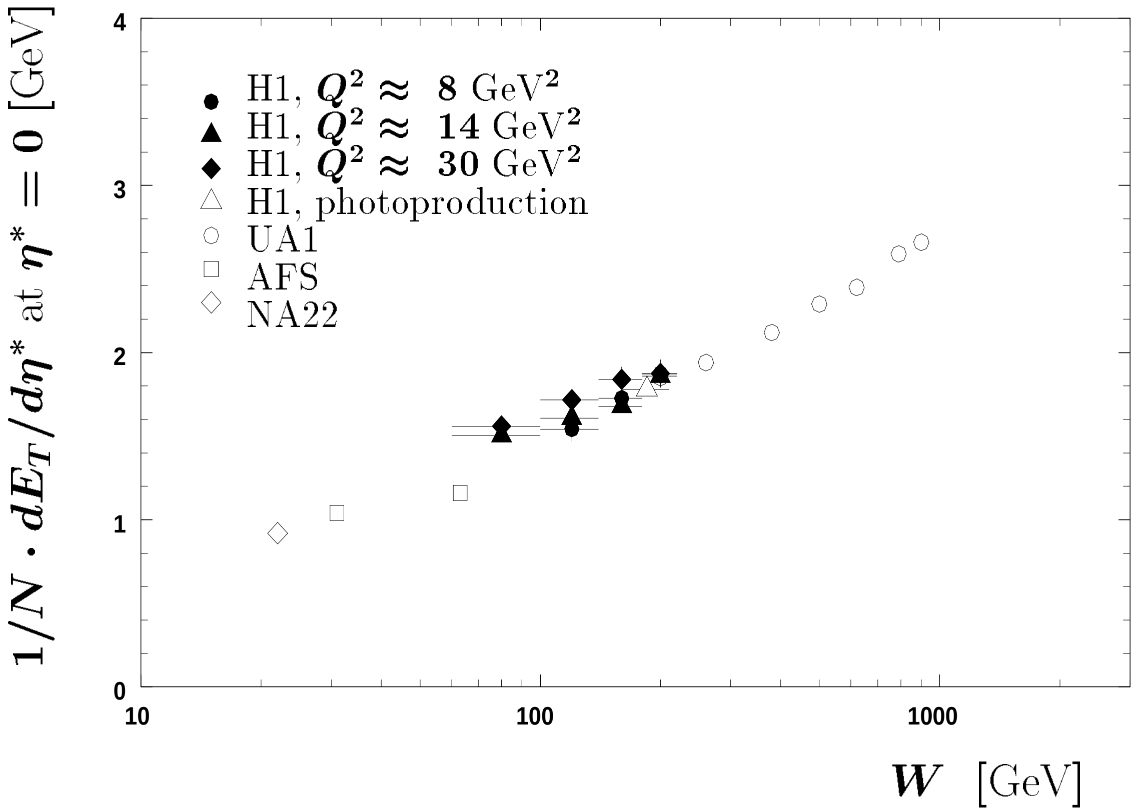

Figure 3: The transverse energy per unit of pseudorapidity in the CMS central region as a function of the hadronic CMS energy. The DIS data are compared with photoproduction data and with data from hadron-hadron collisions ($p\bar{p}$ for UA1; pp for NA22 and AFS). Systematic point-to-point errors of 6% and an overall scale error of 9% for the H1 data are not shown, neither are the global scale uncertainties for the other experiments.

The central region however shows a more universal behaviour, independent of the partonic nature of the colliding particles. It is therefore interesting to compare our measurement with high energy hadron-hadron collisions. In Fig. 3 the transverse energy density, $dE_T/d\eta^*$, at $\eta^* = 0$ is shown for DIS, photoproduction, pp and $\overline{p}p$ interactions as a function of W ($= \sqrt{s}$ for hadron-hadron collisions). The results for DIS include only the data with $Q^2 < 50$ GeV^2, where enough statistics is available to cover a large W (or equivalently y) range. The W dependence of $dE_T/d\eta^*$ observed in DIS processes at low Q^2 (and low x) agrees with the W interpolation between measurements from $p\bar{p}$ [15] and pp [15, 16] collisions. Also the photoproduction data show the same level of E_T for the W value of this data sample. This observation is consistent with the ansatz of the analogy of $\gamma^* p$ interactions with real photon-hadron and hadron-hadron collisions.

In Fig. 4a the distribution of (uncorrected) transverse energy summed over a unit of pseudorapidity in the central region ($-0.5 < \eta^* < 0.5$) is shown for photoproduction and for DIS data ($10 < Q^2 < 100$ GeV^2, $0.3 < y < 0.5$). The comparison shows that in the central region not only the mean E_T, but also the energy spectra themselves, are quite similar. This apparently holds down to very low E_T values, where diffractive dissociation processes are expected to dominate (see peak at $E_T = 0$). Since for $\eta^* = 0$ essentially the same detector regions are used in DIS and photoproduction interactions the agreement is not influenced by detector effects. Following this observation, it is interesting to compare the fraction of diffractive events in photoproduction and DIS.

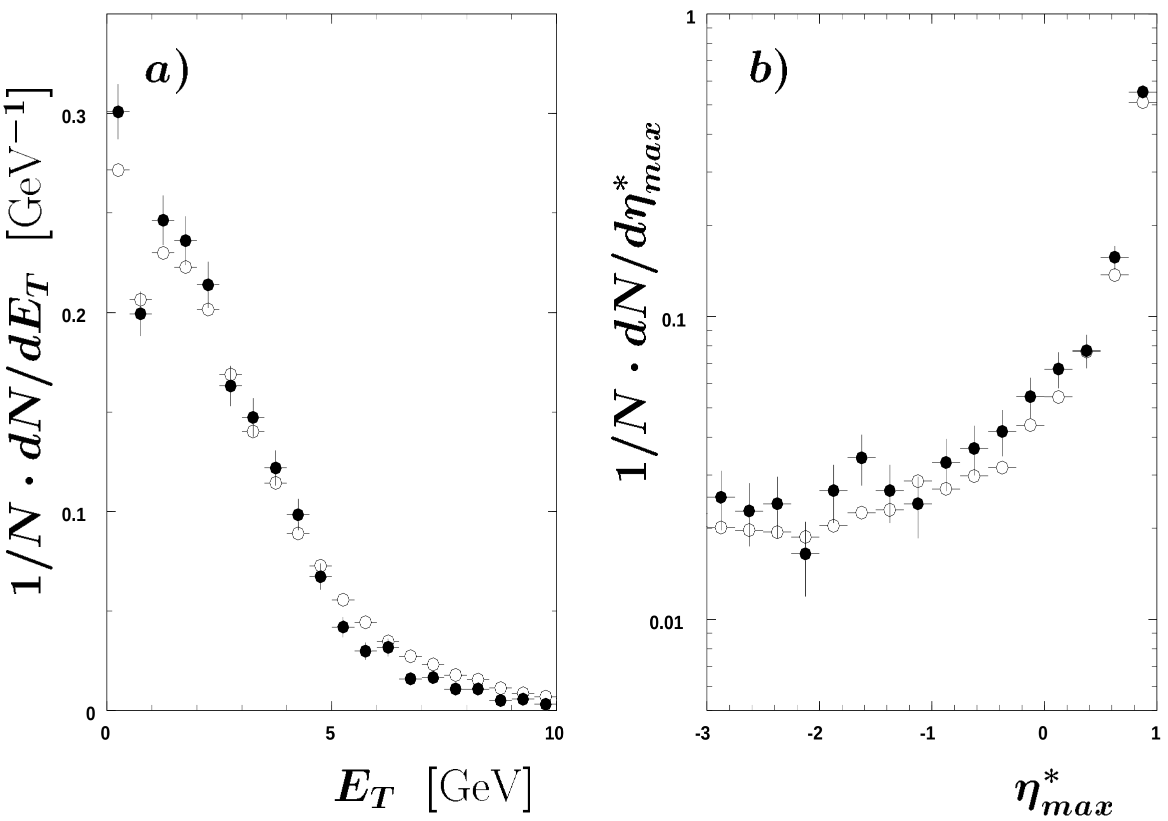

Figure 4: (a) distribution of the uncorrected transverse energy per unit of pseudorapidity in the central region ($-0.5 < \eta^* < 0.5$) , (b) η^*_{max} distribution normalized to the total number of events. Open circles - photoproduction data, full circles - DIS data with $10 < Q^2 < 100$ GeV^2 and $0.3 < y < 0.5$.

An effective way to detect diffractive processes at HERA is via the η^*_{max} variable, which is the maximum pseudorapidity in the $\gamma^* p$ CMS frame, of a reconstructed track or calorimetric cluster with an energy larger than 400 MeV observed in the detector. In diffractive events η^*_{max} indicates the maximum pseudorapidity of secondary hadrons from photon fragmentation and is related to the fraction x_p of the initial proton momentum carried by the diffractively scattered proton via $\eta^*_{max} \sim \ln(1 - x_p) + C$ [17]. The comparison of the η^*_{max} distributions for DIS and photoproduction interactions is shown in Fig. 4b. The figure shows spectra which fall off rapidly from $\eta^*_{max} = 1$ with decreasing η^*_{max}. This part of the spectra can be described by non-diffractive DIS and photoproduction interactions as demonstrated in [1, 18]. For $\eta^*_{max} \sim -1$ the spectra level off to a constant plateau. The events with this and lower η^*_{max} values have been shown to originate predominantly from a diffractive mechanism [19, 18]. Below $\eta^*_{max} < -3$ the photoproduction and DIS data are affected differently by the detector acceptance and therefore not included in this analysis. As a consequence of this cut the low mass resonance region is avoided as well. For diffractive events the distribution $1/N \cdot dN/d\eta^*_{max} \sim (1/\sigma_{tot})(d\sigma/d(1 - x_p))(1 - x_p)$ is expected to be roughly independent of η^*_{max} if the diffractive cross section $d\sigma/d(1 - x_p)$ is approximately inversely proportional to $(1 - x_p)$, see ref. [19]. This lack of dependence of $1/N \cdot dN/d\eta^*_{max}$ on η^*_{max} is itself often taken as the signature of diffraction.

Fig. 4b shows clearly that indeed at low η^*_{max} both for DIS and photoproduction the differential distribution $1/N \cdot dN/d\eta^*_{max}$ is roughly independent of η^*_{max}. Furthermore the relative contribution of the photon high mass diffractive dissociation for photoproduction and DIS interactions is found to be the same to within 15-20%. This agreement is not affected by detector effects since for a given η^*_{max} value largely the same detector regions are explored in

DIS and photoproduction interactions. This observation is at the same level of agreement as measurements made for hadron-hadron interactions, and is in accord with the expectation of approximate factorization of high mass diffractive cross sections, as observed in hadron collisions and explained with triple Regge phenomenology [7]: the ratio of the differential diffractive cross section, $d\sigma/d(1-x_p)$, to the total cross section is approximately independent of the type of dissociating hadron. The fact that this factorization rule also seems to hold for virtual photon interactions gives an additional argument in favour of the validity of a universal hadron-like description of low-x DIS, real photoproduction, and hadron-hadron collisions.

Conclusions

The comparison of low-x DIS data and photoproduction at the ep collider HERA reveals striking similarities in the energy flow of the hadronic final state and relative rate of high mass diffractive dissociation of the photon. The W dependence of the transverse energy density in the central rapidity region is found to be similar to that seen in high energy hadron-hadron collisions. These findings are consistent with the hadronic picture of the photon which can therefore be considered to be complementary to the conventional deep-inelastic scattering picture, even at large Q^2 values. This picture gives a description of the transition region from the high Q^2 perturbative region to the low Q^2 non-perturbative region, and provides a basis for a universal description of hadron-hadron, real photon-hadron and virtual photon-hadron high energy interactions.

References

[1] H1 Collab., T. Ahmed et al., Nucl. Phys. B429 (1994) 477.

[2] ZEUS Collab., M. Derrick et al., Phys. Lett. B315 (1993) 481.

[3] NMC Collab., P. Amaudruz et al., Z. Phys. C51 (1991) 387;
E665 Collab., M.R. Adams et al., Phys. Rev. Lett. 68 (1992) 3266.

[4] B.L. Ioffe, Phys. Lett. B30 (1969) 123.

[5] V. Del Duca, S.J. Brodsky and P. Hoyer, Phys. Rev. D46 (1992) 931.

[6] J.D.Bjorken, SLAC Summer school SLAC-167 (1973) 1.

[7] K. Goulianos, Phys. Rep. 101 (1983) 169.

[8] H1 Collab., T. Ahmed et al., Nucl. Phys. B439 (1995) 471;
H1 Collab., T. Ahmed et al., Phys. Lett. B346 (1995) 415;
H1 Collab., T. Ahmed et al., Nucl. Phys. B445 (1995) 195.

[9] H1 Collab., I. Abt et al., DESY preprint 93-103 (1993), to be published in Nucl. Instr. and Meth.

[10] R. Engel, Proceedings of the XXIXth Recontre de Moriond (1994) 321.

[11] L. Lönnblad, Computer Phys. Comm. 71 (1992) 15.

[12] G. Ingelman, Proc. HERA workshop, Eds. W. Buchmüller and G. Ingelman, Hamburg (1991) Vol. 3, 1366.

[13] H1 Collab., S. Aid et al., Phys. Lett. B356 (1995) 118.

[14] S. Brodsky et al., Phys Rev. D50 (1994) 3134.

[15] UA1 Collab., C. Albajar et al., Nucl.Phys. B335, (1990) 261.

[16] A. De Roeck, Inclusive Particle Production in Hadron-Proton Interactions at 250 GeV/c, Phd. Thesis, Antwerpen (1988).

[17] A.B.Kaidalov, Phys.Rep. 50 (1979) 157.

[18] H1 Collab., T. Ahmed et al., Nucl. Phys. B435 (1995) 3.

[19] H1 Collab., T. Ahmed et al., Phys. Lett. B348 (1995) 681.